nature physics

LETTERS

PUBLISHED ONLINE: 17 OCTOBER 2016 | DOI: 10.1038/NPHYS3904

Directly probing anisotropy in atom–molecule collisions through quantum scattering resonances

Ayelet Klein[1†], Yuval Shagam[1†], Wojciech Skomorowski[2], Piotr S. Żuchowski[3], Mariusz Pawlak[4], Liesbeth M. C. Janssen[5], Nimrod Moiseyev[6], Sebastiaan Y. T. van de Meerakker[7], Ad van der Avoird[7], Christiane P. Koch[2] and Edvardas Narevicius[1*]

Anisotropy is a fundamental property of particle interactions. It occupies a central role in cold and ultracold molecular processes, where orientation-dependent long-range forces have been studied in ultracold polar molecule collisions[1,2]. In the cold collisions regime, quantization of the intermolecular degrees of freedom leads to quantum scattering resonances. Although these states have been shown to be sensitive to details of the interaction potential[3–8], the effect of anisotropy on quantum resonances has so far eluded experimental observation. Here, we directly measure the anisotropy in atom–molecule interactions via quantum resonances by changing the quantum state of the internal molecular rotor. We observe that a quantum scattering resonance at a collision energy of $k_B \times 270$ mK appears in the Penning ionization of molecular hydrogen with metastable helium only if the molecule is rotationally excited. We use state-of-the-art *ab initio* theory to show that control over the rotational state effectively switches the anisotropy on or off, disentangling the isotropic and anisotropic parts of the interaction.

Anisotropy leaves fingerprints on many atomic and molecular processes, but its contribution is difficult to evaluate and quantify at high energies due to the many quantum states needed to describe the process. For example, the effects of anisotropy can be traced to changes in the angular distribution of products in collisions and half-collisions that are detected with advanced ion imaging techniques[9]. Numerous experiments have reported orientation effects including the study of bimolecular processes such as the reactive scattering of $H + D_2$ (ref. 10), and $F + CD_4$ (ref. 11) as well as the inelastic scattering of NO by Ar (ref. 12). Spectroscopic techniques have been successfully used to identify hindered H_2 rotation in an anisotropic potential of van der Waals molecules such as $H_2O + H_2$ and H_2HF complexes[13,14].

In cold and ultracold molecular processes, where the number of accessible quantum states is greatly reduced, anisotropy effects have so far been studied only in fast reactions. It has been shown that the orientation of the long-range dipole–dipole interaction between molecules can be tuned via external electric fields[15]. In KRb molecules this method enabled the observation of rethermalization[1] and the suppression of a bimolecular chemical reaction[2]. In addition, the reaction of $N_2^+ + Rb$ has been shown to be dominated by the anisotropic charge–quadrupole long-range interaction[16]. Similarly, fast Penning ionization reactions have been studied, demonstrating that the rotational state of a molecule defines the type and strength of the effective long-range interaction[17]. These fast processes are fully described by the long-range interactions alone. At short internuclear separations the Penning ionization occurs with unit probability, acting as a perfect absorber and preventing the formation of outgoing waves. In such a case there is no quantization along the internuclear coordinate that precludes the appearance of quantum scattering resonances.

Experiments that are capable of resolving quantum resonance states allow for collision studies with near spectroscopic precision. For example, isotope shifts have been observed in the Penning ionization of molecular hydrogen isotopologues[6]. Similar effects between isotopes were observed in rotational state-to-state cross-sections and linked to quantum scattering resonances appearing at different energies[18]. Feshbach resonances in ultracold anisotropic atom–atom collisions allowed the emergence of chaotic scattering in ultracold Er and Dy to be observed[19].

The emergence of discrete quantized metastable states formed during a cold collision provides a new way to study anisotropy. Instead of recording the angular distribution of the collision products, one can conveniently alter the way anisotropy contributes by choosing different rotational quantum states of the interacting molecules. The sensitivity of the orbiting resonances to the molecular degrees of freedom has been theoretically predicted for the reaction $D + H_2$ (ref. 20), the reactive scattering of $F + H_2$ (ref. 21) and inelastic collisions of $CO + H_2$ (ref. 22), for example. This effect has so far eluded experimental investigation due to the insufficient resolution of individual quantum resonance states[22]. The introduction of merged beam experiments that can reach temperatures as low as 10 mK (refs 3,6) allows for both low enough collision energies and sufficiently high resolutions due to the correlation that develops during the free propagation of a supersonic molecular beam[23]. This merged beam configuration is used in the current collision measurements, as described in the Methods.

Here we demonstrate the dramatic effect of anisotropy on shape resonances in cold Penning ionization reactions of metastable helium in the 2^3S_1 state (He^*) with molecular hydrogen in the rotational ground and first excited states (Fig. 1). In the classical collision regime down to temperatures of several kelvin, H_2 behaves similarly, independent of whether it is in the $j = 0$ or $j = 1$ internal

[1]Department of Chemical Physics, Weizmann Institute of Science, Rehovot 76100, Israel. [2]Theoretische Physik, Universität Kassel, Heinrich-Plett-Straße 40, 34132 Kassel, Germany. [3]Institute of Physics, Faculty of Physics, Astronomy and Informatics, Nicolaus Copernicus University in Torun, Grudziadzka 5, 87-100 Torun, Poland. [4]Faculty of Chemistry, Nicolaus Copernicus University in Toruń, Gagarina 7, 87-100 Toruń, Poland. [5]Institute for Theoretical Physics II, Heinrich-Heine University, Universitaetsstrasse 1, D-40225 Duesseldorf, Germany. [6]Schulich Faculty of Chemistry and Faculty of Physics, Technion-Israel Institute of Technology, Haifa 32000, Israel. [7]Radboud University, Institute for Molecules and Materials, Heijendaalseweg 135, 6525 AJ Nijmegen, Netherlands. [†]These authors contributed equally to this work. *e-mail: edvardas.narevicius@weizmann.ac.il

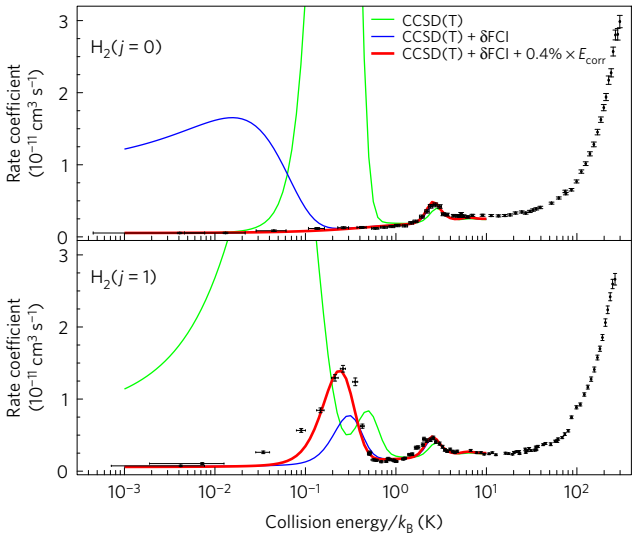

Figure 1 | Experimental and theoretical Penning ionization rate coefficients of H_2 molecules in excited and ground rotational states by He^*. The experimental rate coefficient is shown by the black dots as a function of the mean collision energy in units of temperature. The upper (lower) panel corresponds to H_2 internally in the $j=0$ ($j=1$) rotational quantum state. Two shape resonances are observed below 5 K for the reaction with ortho-H_2 ($j=1$) at 2.37 ± 0.09 K and at 270 ± 20 mK. The $j=1$ lower-energy resonance state corresponds asymptotically to the partial wave $l=3$, whereas the second resonance, which appears both for $j=0$ and $j=1$, corresponds asymptotically to the $l=4$ partial wave. In the reaction with para-H_2 ($j=0$), the $l=3$ resonance is absent, whereas the difference in energy of the $l=4$ resonance cannot be distinguished from the $j=1$ case. The results of state-of-the-art first-principles calculations for the reaction with the ground ($j=0$) and excited ($j=1$) rotational states are depicted by the green, blue and red curves in both panels. The interaction potential obtained with [CCSD(T)/aug-cc-pV6Z+mid-bond, green] alone erroneously predicts a low-energy resonance for para-hydrogen ($j=0$) and two low-energy resonances for ortho-hydrogen ($j=1$). Including the FCI/aug-cc-pVQZ correction (blue) allows for agreement down to collision energies corresponding to a few hundred millikelvin. Further improvement of the interaction potential is achieved by uniformly scaling the correlation energy by 0.4% (red), resulting in excellent agreement with the measured resonance positions and the overall behaviour of the rate coefficient down to the lowest collision energies probed in the experiment. The calculated rate coefficients are convoluted with the experimental resolution (8 mK) for the lowest collision energies. The error bars indicate the standard error in the rate coefficient and the collision energy, calculated according to 500 measurements per data point.

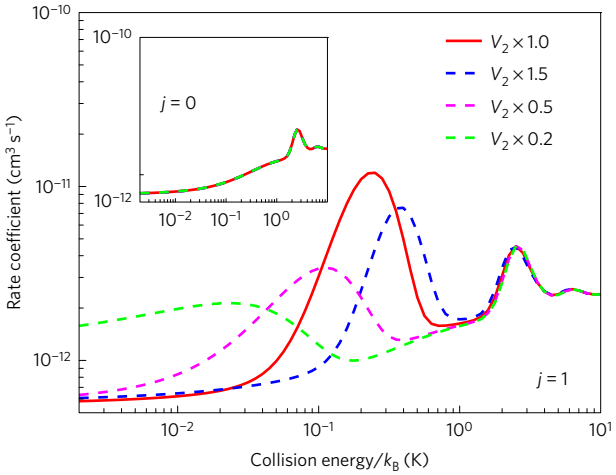

Figure 2 | The theoretical rate coefficients of $He^* + H_2$ in the first excited rotational state ($j=1$) for different scaling factors of the leading order anisotropic potential V_2. The rate resulting from the original potential is depicted by the solid red curve, and the scaling of the anisotropic part by a factor of 1.5, 0.5 and 0.2 is depicted by the blue, magenta and green dashed curves, respectively. As the scaling factor decreases the lower-energy resonance position shifts to lower collision energies. The spectroscopic resolution of the resonance positions can serve as a sensitive measure of the anisotropy in the system. The logarithmic inset shows the rate for scaling factors of the anisotropic potential by the same factors for the reaction of $He^* + H_2$ in the ground rotational state ($j=0$). The rate coefficient remains the same for different scaling factors as the anisotropic potential has a limited contribution to this reaction.

rotational state. However, below one Kelvin we observe a striking difference. While a strong shape resonance exists for $j=1$ at a collision energy of $k_B \times 270 \pm 20$ mK, where k_B is the Boltzmann constant, no resonances are observed in this energy range in the case of $j=0$. Using state-of-the-art *ab initio* theory and coupled-channel quantum molecular dynamics we find that the interaction between hydrogen, which is internally in the ground rotational state, and metastable helium is effectively isotropic. This holds for any collision where the interaction anisotropy is small compared with the rotational constant of the molecule. In such a case, the anisotropic part of the interaction potential becomes important only for molecules in an excited rotational state. The wavefunction of rotationally excited H_2 molecules is not spherically symmetric, which causes the anisotropic components of the interaction to come into play, whereas in the rotational ground state, where the wavefunction is spherically symmetric, the contribution of anisotropic components is zero. We show that by accurately measuring the orbiting resonance positions we can independently probe the isotropic and anisotropic parts of the interaction. As the resonance wavefunctions span both the short- and the long-range parts of the potentials, we are able to benchmark first-principles quantum dynamics calculations to within 7×10^{-3} cm^{-1} or 200 MHz precision. This allows for a rigorous comparison with theory and a quantitative evaluation of the different levels of treating electron correlations in electronic structure calculations.

Conveniently, merged beam experiments with molecular hydrogen can be carried out with control over the rotational state of the molecule. A normal molecular hydrogen beam cooled in supersonic expansions consists of 75% ortho-hydrogen and 25% para-hydrogen. It follows from the Pauli principle that the lowest rotational state for para-hydrogen is $j=0$ whereas $j=1$ is the lowest molecular rotational state for ortho-hydrogen. A pure para-hydrogen sample can be prepared by catalytic conversion at cryogenic temperatures, allowing the determination of the state-selected rate coefficient, as has been described previously[17].

In Fig. 1, we compare our experimental data to the results of first-principles calculations. A two-dimensional potential energy surface was obtained with the current gold standard of electronic structure theory, the coupled-cluster method with single, double and approximate non-iterative triple excitations [CCSD(T)], and further refined to include higher order correlation effects. Subsequently, the potential energy surface was used in quantum scattering calculations with reactive boundary conditions at short range[24]. The theoretical results demonstrate that collisions with $j=0$ hydrogen are not sensitive to the anisotropic part of the interaction potential, such that the hydrogen molecule effectively behaves like an atom. Even scaling the anisotropic part, V_2, by 50% does not introduce an observable change in the rate coefficient, as can be seen in the inset in Fig. 2. In stark contrast the $j=1$ hydrogen rate coefficient is very sensitive to the anisotropy, emerging as shifts in the position of the orbiting resonance

for different scaling factors of the anisotropic potential shown in Fig. 2.

The sensitivity of quantum resonance states to small changes in the interaction allows us to make a meaningful comparison of different levels of treating electron correlations in *ab initio* theory (Fig. 1). In fact, the interaction potential obtained with the 'bare' CCSD(T)/aug-cc-pV6Z+mid-bond method is not accurate enough to reproduce the low-energy resonances for collisions with both $j=0$ and $j=1$ H_2 (see the green curves in Fig. 1). To account for higher-order electron correlation effects, the full configuration interaction (FCI/aug-cc-pVQZ) contribution beyond CCSD(T) has been calculated and added to the potential. The FCI-corrected potential energy surface performs significantly better (blue curves in Fig. 1), in particularly for collisions with $H_2(j=1)$. However, it still erroneously predicts a resonance in the millikelvin range for $H_2(j=0)$. To further improve the theoretical model, we have uniformly scaled the correlation energy. This is motivated by the fact that incompleteness of the orbital basis set is the main source of error in the *ab initio* calculations. It particularly affects the correlation energy, whereas the Hartree–Fock energy is almost fully converged in the aug-cc-pV6Z basis set (see Methods for details). In fact, increasing the correlation energy in the interaction potential by merely 0.4% leads to an excellent agreement for the resonance position of $H_2(j=1)$ and confirms absence of this resonance for $H_2(j=0)$ (red curves in Fig. 1). The latter can be understood as follows: scaling the correlation energy by 0.4% corresponds to increasing the depth of the isotropic potential by around 0.1 cm^{-1}. This shifts the erroneous resonance obtained with CCSD(T) and CCSD(T) + δFCI down such that it becomes a truly bound state and does not affect the reaction rate.

A similar comparison of the different levels of theory and experiment could in principle also be performed using rovibrational spectroscopy of bound states. However, while spectroscopic methods measure the spacings between rovibrational states with high precision, these spacings are not sensitive to a global energy shift of the potential. In collisional spectroscopy the spectrum emerges above the dissociation threshold enabling the measurement of the energies of quasi-bound states on an absolute scale. Thus changes in the effective well depth due to the anisotropy are more pronounced in absolute scale measurements of the spectrum (Fig. 3).

To qualitatively understand the role of anisotropy, it is convenient to consider the effective adiabatic interaction potentials. To this end, the interaction potential is expanded into two terms: $V_0(R)$, the isotropic term where R is the interparticle separation and $V_2(R)P_2(\cos\theta)$, which describes the angular dependence to first order, where θ is the polar angle between the axis of the H_2 molecule and the axis joining the H_2 centre of mass with the He atom. We use an adiabatic theory[25] inspired by previous works[26,27] to construct effective potential curves that conserve the total angular momentum J. These potentials asymptotically correlate with a well-defined rotational state of $H_2(j)$ and a well-defined collisional angular momentum, that is, partial wave l. The anisotropy, $V_2(R)$, is small in our case compared with the rotational constant for all collision distances, such that mixing of the rotational states of the same parity in the H_2 molecule is negligible. Figure 3 compares the three adiabatic potentials that support the lower-energy resonance state that asymptotically correlates with $j=0$ and $j=1$ H_2 and orbital angular momentum (partial wave) $l=3$. The black curve corresponding to $J=3$ and $j=0$ H_2 is identical to the isotropic part of the interaction potential and includes the centrifugal term. It is deep enough to support a single bound state just below the threshold with a binding energy of $k_B \times 0.01$ K, as shown in the inset of Fig. 3. In the case of $j=1$ H_2, the anisotropy is responsible for reducing the well depth of the corresponding $J=3$ effective potential, shown in red, enough to raise the bound state above the dissociation threshold (Fig. 3 inset). This state is located below the top of the centrifugal barrier, and is accessible via tunnelling in scattering experiments at a collision energy of $k_B \times 270$ mK. The grey adiabat in Fig. 3 represents two nearly degenerate effective potential curves with the total angular momentum of $J=2$ and $J=4$ and $j=1$ H_2. Both potentials do not support resonances and have bound levels at $k_B \times 0.18$ K below the dissociation threshold. Following a similar procedure, one can show that the higher-energy resonance, appearing for $j=0$ as well as $j=1$, asymptotically correlates with partial wave $l=4$.

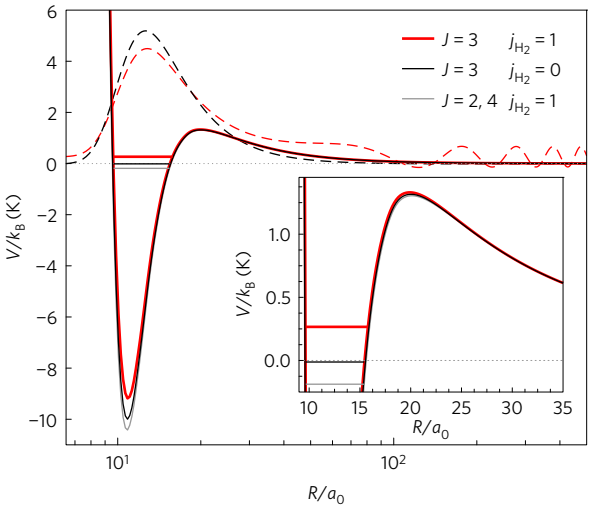

Figure 3 | Effective potential curves for the reaction of He^* and H_2 in the ground and excited rotational states. The potential curves are presented as a function of the He^*–H_2 distance in units of bohr radii (a_0). All of the curves are asymptotically correlated to partial wave $l=3$ and calculated according to adiabatic theory[25]. The adiabatic potentials shown in red and black correspond to the total angular momentum $J=3$. The potential of $j=0$ supports one bound state, located below the dissociation threshold at $k_B \times 0.01$ K. The contribution of the anisotropic part of the potential in the case of $j=1$ (red curve) causes a reduction of the well depth. This reduction is sufficient to shift the bound state by ~0.3 K placing it above the dissociation threshold (see the zoomed-in region in the inset), as depicted by the horizontal solid red line, leading to the resonance at 270 mK in the reaction rate coefficient of $He^* + H_2$ in the excited rotational state ($j=1$). The grey curve corresponds to two nearly degenerate effective potential curves with a total angular momentum of $J=2$ and $J=4$ and with $j=1$ H_2. They support bound states at $k_B \times 0.18$ K below the dissociation threshold and no quasi-bound states. The bound and quasi-bound state wavefunctions for total angular momentum $J=3$ are depicted by the black and red dashed curves, respectively. The resonance state wavefunction spans both the short- and the long-range part of the potential and can therefore be probed in collision experiments.

Orbiting resonances amplify minute differences in particle interactions, making them easily detectable in cold collision experiments provided that the energy resolution is sufficiently high. They are a manifestation of the quantization of the intermolecular degrees of freedom, which form a wave matter analogue of an optical cavity. Quantum resonances thus provide an ideal probe to illuminate the different contributions to particle interactions with a sensitivity that is a challenge for current state-of-the-art *ab initio* theory. The sensitivity of quantum resonances to the internal state of a molecule can be exploited in many experiments. Changing the rotational state of a molecule effectively switches the anisotropy of the interparticle interaction on and off, shifts resonance positions and thus dramatically changes the collisional cross-section. Such control over collisional properties can be critical to the success of molecular cooling methods that rely on collisions, such as evaporative or sympathetic cooling.

Methods

Methods, including statements of data availability and any associated accession codes and references, are available in the online version of this paper.

Received 3 May 2016; accepted 31 August 2016; published online 17 October 2016

References

1. Ni, K.-K. *et al*. Dipolar collisions of polar molecules in the quantum regime. *Nature* **464,** 1324–1328 (2010).
2. de Miranda, M. H. G. Controlling the quantum stereodynamics of ultracold bimolecular reactions. *Nat. Phys.* **7,** 502–507 (2011).
3. Henson, A. B., Gersten, S., Shagam, Y., Narevicius, J. & Narevicius, E. Observation of resonances in Penning ionization reactions at sub-kelvin temperatures in merged beams. *Science* **338,** 234–238 (2012).
4. Chefdeville, S. *et al*. Observation of partial wave resonances in low-energy O_2-H_2 inelastic collisions. *Science* **341,** 1094–1096 (2013).
5. Costes, M. & Naulin, C. Observation of quantum dynamical resonances in near cold inelastic collisions of astrophysical molecules. *Chem. Sci.* **7,** 2462–2469 (2016).
6. Lavert-Ofir, E. *et al*. Observation of the isotope effect in sub-kelvin reactions. *Nat. Chem.* **6,** 332–335 (2014).
7. Vogels, S. N. *et al*. Imaging resonances in low-energy NO–He inelastic collisions. *Science* **350,** 787–790 (2015).
8. Bergeat, A., Onvlee, J., Naulin, C., van der Avoird, A. & Costes, M. Quantum dynamical resonances in low-energy CO($j=0$) + He inelastic collisions. *Nat. Chem.* **7,** 349–353 (2015).
9. Ashfold, M. N. R. *et al*. Imaging the dynamics of gas phase reactions. *Phys. Chem. Chem. Phys.* **8,** 26–53 (2006).
10. Kitsopoulos, T. N., Buntine, M. A., Baldwin, D. P., Zare, R. N. & Chandler, D. W. Reaction product imaging: the H + D_2 reaction. *Science* **260,** 1605–1610 (1993).
11. Lin, J. J., Zhou, J., Shiu, W. & Liu, K. State-specific correlation of coincident product pairs in the F + CD_4 reaction. *Science* **300,** 966–969 (2003).
12. Kohguchi, H., Suzuki, T. & Alexander, M. H. Fully state-resolved differential cross sections for the inelastic scattering of the open-shell NO molecule by Ar. *Science* **294,** 832–834 (2001).
13. van der Avoird, A. & Nesbitt, D. J. Rovibrational states of the H_2O–H_2 complex: an *ab initio* calculation. *J. Chem. Phys.* **134,** 044314 (2011).
14. Lovejoy, C. M., Nelson, D. D. & Nesbitt, D. J. Hindered internal rotation in jet cooled H_2 HF complexes. *J. Chem. Phys.* **87,** 5621–5628 (1987).
15. Carr, L. D., DeMille, D., Krems, R. V. & Ye, J. Cold and ultracold molecules: science, technology and applications. *New J. Phys.* **11,** 055049 (2009).
16. Hall, F. H. J. & Willitsch, S. Millikelvin reactive collisions between sympathetically cooled molecular ions and laser-cooled atoms in an ion-atom hybrid trap. *Phys. Rev. Lett.* **109,** 233202 (2012).
17. Shagam, Y. *et al*. Molecular hydrogen interacts more strongly when rotationally excited at low temperatures leading to faster reactions. *Nat. Chem.* **7,** 921–926 (2015).
18. Hauser, D. *et al*. Rotational state-changing cold collisions of hydroxyl ions with helium. *Nat. Phys.* **11,** 467–470 (2015).
19. Maier, T. *et al*. Emergence of chaotic scattering in ultracold Er and Dy. *Phys. Rev. X* **5,** 041029 (2015).
20. Simbotin, I. & Côté, R. Effect of nuclear spin symmetry in cold and ultracold reactions: D + para/ortho-H_2. *New J. Phys.* **17,** 065003 (2015).
21. Lique, F., Li, G., Werner, H.-J. & Alexander, M. H. Communication: non-adiabatic coupling and resonances in the F + H_2 reaction at low energies. *J. Chem. Phys.* **134,** 231101 (2011).
22. Chefdeville, S. *et al*. Experimental and theoretical analysis of low-energy CO + H_2 inelastic collisions. *Astrophys. J.* **799,** L9 (2015).
23. Shagam, Y. & Narevicius, E. Sub-Kelvin collision temperatures in merged neutral beams by correlation in phase-space. *J. Phys. Chem. C* **117,** 22454–22461 (2013).
24. Janssen, L. M. C., van der Avoird, A. & Groenenboom, G. C. Quantum reactive scattering of ultracold NH($X^3\Sigma^-$) radicals in a magnetic trap. *Phys. Rev. Lett.* **110,** 063201 (2013).
25. Pawlak, M., Shagam, Y., Narevicius, E. & Moiseyev, N. Adiabatic theory for anisotropic cold molecule collisions. *J. Chem. Phys.* **143,** 074114 (2015).
26. Holmgren, S. L., Waldman, M. & Klemperer, W. Internal dynamics of van der Waals complexes. I. Born–Oppenheimer separation of radial and angular motion. *J. Chem. Phys.* **67,** 4414–4422 (1977).
27. Scribano, Y., Faure, A. & Lauvergnat, D. Rotational excitation of H_2O by para-H_2 from an adiabatically reduced dimensional potential. *J. Chem. Phys.* **136,** 094109 (2012).

Acknowledgements

The authors acknowledge financial support from the European Commission through ERC Grant EU-FP7-ERC-CoG 1485 QuCC. Additional financial support from the German–Israeli Foundation (Grant no. 1254), the COST Action MOLIM (CM1405) and the Polish National Science Center (Grant no. DEC-2012/07/B/ST2/00235) is acknowledged. This research was also supported by the I-Core (the Israeli Excellence Center) 'Circle of Light', by the Israel Science Foundation Grant nos 298/11 and 1530/15.

Author contributions

All authors contributed to all aspects of this work.

Additional information

Reprints and permissions information is available online at www.nature.com/reprints. Correspondence and requests for materials should be addressed to E.N.

Competing financial interests

The authors declare no competing financial interests.

Methods

The experimental set-up, which has been discussed previously[3,6,17], consists of two supersonic beams that are generated by pulsed Even–Lavie valves[28] placed at a relative angle of 10°. The straight beam consists of noble gas mixtures of H_2. The second beam consists of ^{4}He, excited to He* using a dielectric barrier discharge[29] that is located at the exit of the valve and is merged with the straight beam using a 20 cm magnetic guide, leading to zero relative angle between the beams at the detection region. The He* beam velocity is kept constant at 870 m s^{-1} while the H_2 beam velocity is tuned by changing the valve temperature and seeding the H_2 in noble carrier gas mixtures. The collision energy is determined by the relative mean velocity between the beams and the velocity distribution of each beam ranging from 300 K to 10 mK (ref. 23).

The metastable He beam is characterized using an on-axis multichannel plate. The H_2 beam is characterized using a time-of-flight mass spectrometer (TOF-MS)[30], which contains an additional ionization element. The TOF-MS is positioned perpendicular to the beams' propagation, operating in a multi-pulsed mode, at 4 μs intervals. The reaction product ions are detected with the TOF-MS with the ionization element turned off, while the neutral molecules are characterized with the ionization element turned on. The relative rate coefficient is calculated according to the ratio between the measured signals of the products and reactants at each time interval. The rate coefficient is normalized to an absolute scale according to room-temperature thermal rate measurement of $He(2^3S_1) + H_2$ (ref. 31).

The para-H_2 sample is prepared by liquefying normal H_2 in liquid helium while in contact with the paramagnetic catalyst nickel sulfate. The sample is examined by resonance-enhanced multiphoton ionization followed by detection with the TOF-MS to determine its purity, showing that more than 98% of the H_2 is in the ground rotational state, as previously described in detail[32].

Rate coefficients were obtained by carrying out coupled-channel quantum reactive scattering calculations using a method[24] in which only the reactant configuration is explicitly considered, and knowledge of the real value of the interaction energy is sufficient. This approach is based on the assumption that the reaction proceeds irreversibly once the reactants reach a sufficiently short interparticle distance R_c, the 'capture radius'; and reactive collisions are simulated by imposing appropriate short-range boundary conditions. Such a quantum capture approach is particularly suitable for describing a chemi-ionization process because of its irreversibility and strongly exoenergetic character, which implies that the total rate coefficient is exclusively determined by the dynamics in the entrance channel of the reaction. As the real-valued Born–Oppenheimer interaction potential between He* and H_2 does not include any coupling with the ionization continuum, $He + H_2^+ + e^-$, we modified the purely repulsive wall of the potential, assuming that the isotropic part $V_0(R)$ is constant (V_c) at short intermolecular distance ($R < R_c$) and equal to the energy released in the ionization process, that is, $V_0(R) \equiv V_c = -3.646$ eV if $R \leq R_c$. This results in a barrier at short range and allows for the loss of the flux into the reactive channels via quantum tunnelling.

Close-coupling quantum scattering calculations were performed separately for collisions of He* with para-$H_2(j=0)$ and with ortho-$H_2(j=1)$. The angular basis functions were constructed as products of the rotational state of the H_2 molecule and the partial wave describing the orbital motion of the whole complex, and were symmetry-adapted to values of the total angular momentum J and parity. The basis set was restricted to even or odd rotational states of H_2 for collisions with para-H_2, or ortho-H_2, respectively. For collision energies up to 10 K, the basis set that yielded fully converged cross-sections included all of the relevant functions with $j \leq 4$ and $J < 8$. The scattering wave functions were propagated from $7.0a_0$ to $200a_0$ by means of a renormalized Numerov propagator. The capture radius was determined by the condition that the elastic cross sections are fully converged; choosing a smaller R_c only results in a homogeneous scaling of the reaction rate coefficients, as does a modification of V_c. Short-range and asymptotic boundary conditions were imposed afterwards, as described in the original paper[24]. The calculated rate coefficients are convoluted with the experimental resolution, which is 8 mK for the lowest collision energies.

The potential energy surface was obtained using the counterpoise corrected supermolecular method in which the interaction energy is obtained as the difference of the total energy of the dimer ($He^* + H_2$) and the total energies of the monomers, calculated in the basis set of the dimer with basis functions placed at the position of the interacting partner with charges set to zero. As the $He^* + H_2$ system is not the actual triplet ground state of the system (which is $He(1^1S) + {}^3\Sigma$ excited H_2) we have employed the maximum overlap method[33,34] with the orbitals corresponding to the isolated $He^* + H_2$ potential with an appropriate occupancy of $1s^1 2s^1 \sigma_g^2$ as the starting point. The spin-restricted coupled-cluster method with single and double excitations with non-iterative corrections to triple excitations [CCSD(T)] in a very large basis set, now considered the gold standard of quantum chemistry, was employed, using the MOLPRO suite of codes[35]. The aug-mcc-pVXZ family for the hydrogen atom[36] and the aug-cc-pVXZ family optimized for the triplet state of the metastable helium dimer[37] were employed, where $X = 4, 5, 6, 7$ stands for the cardinal number, which corresponds to the highest angular momentum, equal to $l = 3, 4, 5, 6$, respectively. To better account for the dispersion interaction we have also used a set of mid-bond functions located between the centre of mass of the H_2 molecule and the He atom. These were obtained from polarization functions of hydrogen atom basis sets. The potential used in the subsequent scattering calculations was obtained with the aug-cc-pV6Z basis set. At large intermolecular separations, between $R = 16a_0$ and $R = 20a_0$, it was smoothly connected to the analytic long-range potential, employing a switching function[38] and the long-range coefficients (C_6 and C_8) of ref. 39. The interatomic distance of the H_2 molecule was set to $1.4487a_0$, which corresponds to the expectation value of the interatomic separation in the ground vibrational state of the hydrogen molecule. To ensure a proper convergence of the expansion into Legendre polynomials, the potential was calculated from 0° to 90° with a step of 15°. The projection onto Legendre polynomials was performed with a published integration procedure[38].

The interaction energy was corrected beyond CCSD(T) with the correction obtained as the difference between the coupled-cluster method with fourth-fold excitations (CCSDTQ) and CCSD(T) in the same basis set. Owing to the enormous numerical cost, CCSDTQ calculations, which are equivalent to FCI for a four-electron system and exact for a given basis set, were performed only for linear- and T-shape geometries, with a smaller basis set, aug-cc-pVQZ and no mid-bond functions, using the CFOUR package (http://www.cfour.de) interfaced with the MRCC programme[40]. The dominant source of uncertainty of the potential energy surface is incompleteness of the basis set, whereas relativistic effects and the diagonal Born–Oppenheimer (DBO) correction were found to be negligible: relativistic effects, estimated by calculating the scalar relativistic perturbation correction (mass velocity and one-electron Darwin term) are of the order of 0.01 cm^{-1} in the global minimum with a well depth of 14.30 cm^{-1} at $10.5a_0$. The DBO correction was obtained as the difference between the corrections for the dimer and infinitely separated monomers for T-shape and L-shape geometries, calculated with the aug-cc-pVQZ basis set and the Hartree–Fock wavefunction (it is not sensitive to the size of the basis set nor the quality of the wavefunction). The contribution of the DBO correction to V_0 is 0.044 cm^{-1} in the global minimum. The incompleteness of the basis set only affects the correlation energy, whereas the Hartree–Fock interaction energy is converged to within 0.01 cm^{-1} in our calculations. Truncation of the basis set results in a shallower potential and an inner turning point that is slightly shifted towards larger intermolecular distances. The limit of the basis set is estimated assuming a convergence pattern $A + BX^{-3}$ or $A + BX^{-3} + CX^{-5}$ for singlet systems and $A + BX^{-5}$ for triplet helium as the correlation energy was found to converge with the cardinal number as X^{-3} for singlet electron pairs and as X^{-5} for triplet pairs[41,42]. The correlation energy in the H_2 and He* monomers are very different in magnitude (9,031 ± 1 cm^{-1} compared with 214.7 ± 0.01 cm^{-1}). For the total system, the basis set limit for the CCSD(T) calculations in the global minimum extrapolated from the aug-cc-pV6Z and aug-cc-pV7Z basis sets (in the latter case we could afford for such calculations for single geometry) is −14.62 cm^{-1}, whereas extrapolation from the $X = 5, 6, 7$ basis set yields the limit −14.42 cm^{-1}. As a conservative estimate, we take the difference between the potential obtained in aug-cc-pV6Z and the basis set limit extrapolated from $X = 6, 7$ as the uncertainty of the potential.

Data availability. The data that support the plots within this Letter and other findings of this study are available from the corresponding author upon reasonable request.

References

28. Even, U., Jortner, J., Noy, D., Lavie, N. & Cossart-Magos, C. Cooling of large molecules below 1 K and He clusters formation. *J. Chem. Phys.* **112,** 8068–8071 (2000).
29. Luria, K., Lavie, N. & Even, U. Dielectric barrier discharge source for supersonic beams. *Rev. Sci. Instrum.* **80,** 104102 (2009).
30. Wiley, W. C. & McLaren, I. H. Time-of-flight mass spectrometer with improved resolution. *Rev. Sci. Instrum.* **26,** 1150–1157 (1955).
31. Veatch, G. E. & Oskam, H. J. Collision processes occurring in decaying plasmas produced in helium-hydrogen mixtures. *Phys. Rev. A* **8,** 389–396 (1973).
32. Pratt, S. T., Dehmer, P. M. & Dehmer, J. L. Photoionization of excited molecular states. H_2 $C^1\Pi_u$. *Chem. Phys. Lett.* **105,** 28–33 (1984).
33. Gilbert, A. T. B., Besley, N. A. & Gill, P. M. W. Self-consistent field calculations of excited states using the maximum overlap method (MOM). *J. Phys. Chem. A* **112,** 13164–13171 (2008).
34. Hapka, M., Chałasiński, G., Kłos, J. & Żuchowski, P. S. First-principle interaction potentials for metastable He(^{3}S) and Ne(^{3}P) with closed-shell molecules: application to Penning-ionizing systems. *J. Chem. Phys.* **139,** 014307 (2013).
35. Werner, H.-J., Knowles, P. J., Knizia, G., Manby, F. R. & Schütz, M. Molpro: a general-purpose quantum chemistry program package. *WIREs Comput. Mol. Sci.* **2,** 242–253 (2012).

36. Mielke, S. L., Garrett, B. C. & Peterson, K. A. A hierarchical family of global analytic Born–Oppenheimer potential energy surfaces for the H + H_2 reaction ranging in quality from double-zeta to the complete basis set limit. *J. Chem. Phys.* **116,** 4142 (2002).
37. Przybytek, M. & Jeziorski, B. Bounds for the scattering length of spin-polarized helium from high-accuracy electronic structure calculations. *J. Chem. Phys.* **123,** 134315 (2005).
38. Janssen, L. M. C., Groenenboom, G. C., van der Avoird, A., Żuchowski, P. S. & Podeszwa, R. *Ab initio* potential energy surfaces for $NH(^3\Sigma^-)$-$NH(^3\Sigma^-)$ with analytical long range. *J. Chem. Phys.* **131,** 224314 (2009).
39. Bishop, D. M. & Pipin, J. Dipole, quadrupole, octupole, and dipole–dipole–quandrupole polarizabilities and second hyperpolarizabilities at real and imaginary frequencies for helium in the 2^3S state: Dispersion-energy coefficients for interactions between He(2^3S) and H(1^2S), He(1^1S) He(2^3S), or $H_2(X^1\Sigma_g^+)$. *Int. J. Quantum Chem.* **47,** 129–134 (1993).
40. Rolik, Z., Szegedy, L., Ladjánszki, I., Ladóczki, B. & Kállay, M. An efficient linear-scaling CCSD(T) method based on local natural orbitals. *J. Chem. Phys.* **139,** 094105 (2013).
41. Helgaker, T., Klopper, W., Koch, H. & Noga, J. Basis-set convergence of correlated calculations on water. *J. Chem. Phys.* **106,** 9639–9646 (1997).
42. Kutzelnigg, W. & Morgan, J. D. Rates of convergence of the partial-wave expansions of atomic correlation energies. *J. Chem. Phys.* **96,** 4484–4508 (1992).